Green Chemistry

PAPER

View Article Online
View Journal

Cite this: DOI: 10.1039/d6gc00485g

Towards scalable production of bound extracellular polymeric substances (B-EPS): autoclave hydrothermal extraction coupled with solvent-free ultrafiltration

Ivana Mendonça, [a,b,c] Filipa Rodrigues, [a,b] Marisa Faria, [a,b]* Juan L. Gómez Pinchetti, [d] Artur Ferreira [c] and Nereida Cordeiro [a,b]*

Bound extracellular polymeric substances (B-EPS) are extracellular polysaccharides tightly attached to cyanobacterial and microalgal cell surfaces, representing a high-value class of biopolymers with industrial potential. Selective extraction is technically challenging due to strong adhesion to the cell wall and potential co-extraction of soluble EPS. Conventional methods can be chemically aggressive and may involve high energy and/or solvent inputs, making solvent-free extraction routes desirable. In this work, four hydrothermal extraction techniques (reflux, autoclave, ultrasonic bath, and microwave) were evaluated for their ability to recover B-EPS from the marine cyanobacterium *Chroococcus submarinus* (BEA 1200B), followed by a harmonised ultrafiltration step. Each method was assessed for extraction efficiency and its impact on bulk descriptors (inorganic carry-over, ATR-FTIR, zeta potential, and thermal profiles) and morphology. Among the methods tested, autoclave extraction demonstrated the highest performance, yielding up to 2.5 times more B-EPS than the other methods and showing reduced inorganic carry-over after purification. Across all methods, the purified B-EPS fractions exhibited broadly comparable bulk profiles under the applied analytics. Response Surface Methodology (RSM) applied to the autoclave system identified temperature and extraction time as key variables; optimal conditions (biomass-to-solvent ratio 1 : 20 (w/v), 130 °C, 16 min) enabled >90% recovery. Coupling autoclave extraction with solvent-free ultrafiltration avoids solvent precipitation and the use of hazardous reagents, enabling desalting and removal of low-molecular-weight components. Using a photosynthetic marine strain supports seawater cultivation and biogenic CO_2 uptake, aligning the workflow with carbon-mitigation goals.

Received 23rd January 2026,
Accepted 5th February 2026

DOI: 10.1039/d6gc00485g

rsc.li/greenchem

Green foundation

1. This work advances green extraction of cell-associated polysaccharides by combining water-only hydrothermal processing with ultrafiltration desalting, avoiding organic-solvent precipitation and added chemical reagents while enabling selective recovery of cyanobacterial B-EPS.
2. Across the evaluated routes, autoclaving delivered the highest recovered mass (up to 2.5-fold *vs.* reflux/ultrasonication), and RSM optimisation enabled >90% recovery under short residence times and scalable operating conditions.
3. Further greening can be achieved by reporting energy/PMI/*E*-factor at pilot scale, implementing heat integration and permeate reuse, and assessing whether avoiding freeze-drying (direct use of aqueous concentrates) preserves functionality while reducing energy demand.

Introduction

Bound extracellular polymeric substances (B-EPS), also referred to as capsular or cell-associated EPS, are predominantly extracellular polysaccharides that remain tightly associated with the cell surface of a wide range of microorganisms, including heterotrophic bacteria, cyanobacteria, and microalgae. These polymers form cohesive pericellular matrices that can enhance tolerance to environmental stressors such as desiccation, radiation/light exposure, temperature shifts, nutri-

[a]*LB3, Faculty of Science and Engineering, University of Madeira, 9020-105 Funchal, Portugal. E-mail: ncordeiro@staff.uma.pt, marisa.faria@staff.uma.pt*
[b]*CIIMAR, Interdisciplinary Centre of Marine and Environmental Research, University of Porto, 4450-208 Matosinhos, Portugal*
[c]*CICECO, Aveiro Institute of Materials and Águeda School of Technology and Management, University of Aveiro, 3754-909 Águeda, Portugal*
[d]*Spanish Bank of Algae, Institute of Oceanography and Global Change (IOCAG), University of Las Palmas de Gran Canaria, Muelle de Taliarte S/N, Telde, Canary Islands, 35214 Las Palmas, Spain*

ent limitation, and oxidative stress.[1,2] Due to their structural stability, compositional diversity, and functional versatility, B-EPS have attracted increasing interest as renewable biopolymers with significant industrial potential.[3,4]

While B-EPS represent a widespread microbial trait, photosynthetic marine cyanobacteria constitute an especially attractive production platform by combining CO_2 fixation, solar-driven growth, and seawater cultivation with the ability to produce abundant and chemically complex extracellular matrices.[5,6] However, their selective extraction remains technically challenging because of the strong adhesion of B-EPS to the cell envelope and the high risk of co-extraction of soluble EPS (S-EPS), which compromises selectivity and downstream interpretation, and can inflate apparent recovery and confound attribution of measured bulk descriptors to the cell-associated fraction.[5–7] Conventional approaches can be inefficient and/or chemically aggressive, leading to partial polymer degradation, high inorganic carry-over, and limited reproducibility, ultimately restricting their broader application and scalability.[8,9] Although B-EPS and S-EPS may share broadly similar chemical functionalities (*e.g.*, polysaccharidic backbones and carboxylate or sulphate groups), they differ in biological localisation, ecological roles, and extraction behaviour, which makes selective recovery of the cell-associated fraction technically challenging.[5–7] *Chroococcus submarinus* was selected as a model marine cyanobacterium because it produces a conspicuous, cohesive capsular/pericellular matrix, which is operationally associated with the cell-bound fraction, making it particularly suitable for benchmarking selective detachment and solvent-free purification strategies. Cells typically occur as aggregates embedded in a dense mucilaginous envelope, enabling a practical microscopic readout of extracellular matrix redistribution following treatment. Importantly, the main physicochemical constraints addressed here (salt co-extraction, strong B-EPS adhesion, and retention of anionic functionalities inferred from bulk descriptors) are shared by many marine cyanobacteria and EPS-rich microalgae, supporting transferability of the proposed workflow to additional strains, with species-specific optimisation as needed.[6,10,11] A major bottleneck in marine EPS processing is salt contamination, which interferes with downstream analyses and limits product quality; therefore, purification strategies able to remove ions and low-molecular-weight impurities while maintaining comparable bulk signatures are essential.[10,11] Ultrafiltration (UF) provides a solvent-free route for desalting and purification, avoiding drawbacks associated with organic solvent precipitation.[10,11]

This study compares four water-based extraction strategies: reflux, autoclave, ultrasonic, and microwave-assisted treatments, applied to *C. submarinus* to benchmark recovery and selectivity towards the operationally defined bound fraction (cell-associated recovery coupled to UF purification), while assessing bulk signatures through orthogonal analytics. Extracted polymers were subsequently purified by UF as a solvent-free route for desalting and removal of low-molecular-weight impurities. B-EPS were characterised using scanning electron microscopy (SEM), attenuated total reflection Fourier-transform infrared spectroscopy (ATR-FTIR), thermogravimetric analysis (TGA), elemental/ash analysis, and zeta potential, enabling comparative assessment of bulk chemical, thermal, and colloidal descriptors.

All methods were applied to the same starting biomass and evaluated using a harmonised analytical framework, providing a reproducible basis to benchmark extraction performance and to support the development of scalable, water-based processing routes for purified B-EPS suitable for renewable materials applications.[3,12]

Experimental

Cyanobacterial cultivation

The marine cyanobacterium *C. submarinus* (strain BEA 1200B) was obtained from the Spanish Bank of Algae (BEA, Telde, Canary Islands, Spain). Cultivation was performed in ASP-12 medium prepared according to the formulation described by Laroche and Cruz *et al.*, with the complete composition provided in Table S1.[6,10] Cultures were maintained in an Aralab CP500 growth chamber under a 14 : 10 h light/dark photoperiod at 25 ± 2 °C and irradiance of 40 μmol photons m^{-2} s^{-1} supplied by cool-white fluorescent lamps (Osram L 18W840 Lumilux). Temperature and light intensity were continuously monitored using a HOBO® Pendant® MX Temp MX2201 data logger. To ensure reproducibility across extraction experiments, biomass from a homogeneous culture was produced under identical controlled conditions for six months.

B-EPS extraction and purification

All extractions were performed using biomass from a single, homogeneous culture of *C. submarinus* to ensure reproducibility. Before extraction, salt-removal strategies were evaluated to minimise inorganic contamination, which is particularly relevant for marine strains.[10,11] Two approaches were compared: (i) centrifugation at 5000 rpm (3070*g*, 10 min) and (ii) triple washing with distilled water. For subsequent extractions, the washing protocol was adopted to standardise sample preparation across methods. Washed biomass was resuspended in distilled water at a biomass-to-solvent ratio of 1 : 15 (w/v; g mL^{-1}) and subjected to one of four hydrothermal techniques:

(i) Reflux extraction: 105 °C, 15 min;

(ii) Autoclave extraction: 121 °C, 15 min (CertoClav Vacuum Pro 12, nominal mains frequency 50/60 Hz, nominal power of 2500 W, 230 V);

(iii) Ultrasonic extraction: 80 °C, 15 min (Selecta Ultrasons-H ultrasonic bath, nominal frequency 40 kHz, nominal power 1200 W, 230 V, bath mode);

(iv) Microwave extraction: 900 W, 60 s (Moulinex Optimo operating at 900 W, 230 V).

Because these techniques deliver energy differently, operating parameters (temperature/power profiles) are necessarily method-specific; therefore, comparisons were benchmarked

using the same biomass source and fixed biomass-to-solvent ratio, followed by a harmonised UF step.

For microwave treatment, the suspension temperature was recorded immediately before and after irradiation, increasing from room temperature to near-boiling conditions, to report the effective temperature window achieved during heating, with temperature measured immediately after irradiation using a probe/thermometer. For reflux, autoclave and ultrasound treatments, processing time refers to the applied treatment time after reaching the set temperature; for microwave treatment, the processing time corresponds to the irradiation time.

Immediately after extraction, suspensions were manually agitated to promote B-EPS release and centrifuged at 2500 rpm (770*g*, 10 min) to remove residual biomass. The supernatants containing B-EPS were purified by UF using a 100 kDa molecular weight cut-off cassette (Sartorius Vivaflow 50). A sequence of 11 concentration/dilution cycles with bidistilled water was performed until conductivity plateaued (Consort C5020), confirming efficient removal of free salts and low-molecular-weight species (Fig. S1). Retentates were stored at 4 °C for short-term use or freeze-dried at −50 °C (Savant RT 400) and kept at 4 °C until further analysis. A schematic representation of the extraction and purification workflow is shown in Fig. 1.

Chemical and physicochemical analyses

Light microscopy. The presence and distribution of Alcian Blue-stained pericellular/cell-associated matrix features before and after extraction were examined using an optical microscope (Leica DM2700) equipped with a digital camera (Leica DFC450C) and LED illumination (CoolLED pE-300 lite). Samples were stained with Alcian Blue following Rodrigues *et al.*[13] A 1 mg mL^{-1} solution of Alcian Blue 8GN (Sigma-Aldrich A5268) in 0.5 M acetic acid (pH 2.5) was mixed with the sample at a 1 : 1 ratio, incubated for 30 min, and mounted on glass slides for observation. For each condition, images were acquired from multiple fields of view under identical acquisition settings.

Scanning electron microscopy (SEM). Morphological alterations of the biomass and surface-associated extracellular matrix features after extraction were analysed by field-emission SEM (Hitachi SU-70 HR-FESEM). Freeze-dried samples were sputter-coated with carbon (EMITECH K950X), mounted on steel stubs, and imaged at 5 kV and a working distance of 15.6 mm, with magnifications of 80× and 500×.

Thermogravimetric analysis (TGA). Thermal stability and inorganic content were determined using a SETSYS Setaram TGA analyser with a platinum crucible. Freeze-dried B-EPS were heated from ambient temperature to 550 °C at 10 °C min^{-1} under a 20 mL min^{-1} oxygen flow. TGA and derivative (dTG) curves were recorded, and ash content was calculated as the residual mass at 550 °C.

Attenuated total reflection – Fourier transform infrared spectroscopy (ATR-FTIR). Chemical profiles and functional groups were analysed by ATR-FTIR (PerkinElmer Spectrum BX) equipped with a single-bounce Golden Gate ATR cell. Freeze-dried samples of intact biomass, purified B-EPS, and biomass depleted of B-EPS were scanned between 4000 and 500 cm^{-1} (64 scans, 4 cm^{-1} resolution). Spectra were baseline-corrected and normalised for comparative display.

Elemental analysis. Elemental composition (C, H, N, S) was determined using a Truspec 630–200–200 analyser, with combustion and afterburner temperatures of 1075 °C and 850 °C, respectively. C, H, and N were quantified by infrared absorption, and S by thermal conductivity. Oxygen was calculated by difference, considering the sample's ash content: % O = 100 − (% C + % H + % N + % S + % ash).

Zeta potential. Surface charge and colloidal stability were determined by zeta potential measurements using a Zetasizer Nano ZSP (Malvern) in Milli-Q water at 25 °C. Each sample was measured in triplicate, with 100 measurements taken per sample. To reduce variability associated with ionic strength, all samples were analysed after UF and diluted to a comparable conductivity range; therefore, zeta potential values are reported as screening descriptors rather than strictly comparable parameters under fixed ionic strength.

Response surface methodology (RSM)

Optimisation of autoclave extraction parameters was performed using a three-level face-centered central composite design (CCD) in Design-Expert v13 (Stat-Ease, Inc.), with temperature, extraction time, and biomass-to-solvent ratio as independent variables, and B-EPS recovery (%). The design comprised 2^3 factorial points, 2k axial (star) points and replicated centre points (total = 48 runs; Table S2). Model significance

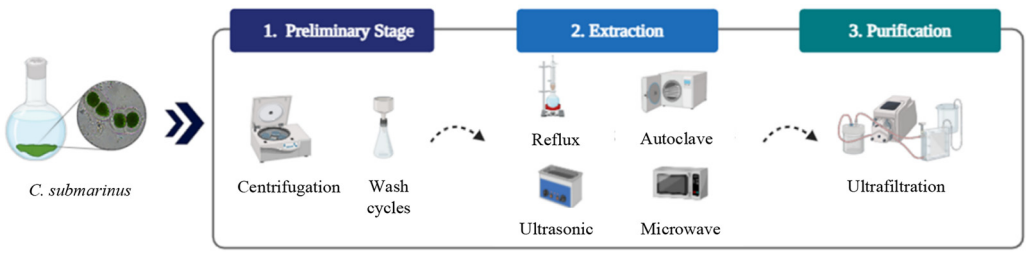

Fig. 1 General overview of the extraction and purification steps.

was evaluated using ANOVA, which included lack-of-fit testing and residual analysis. At the same time, robustness was assessed using coefficients of determination (R^2) and prediction error metrics, following the approaches of Mendonça *et al.* and Rodrigues *et al.*[14,15]

Statistical analysis

All experiments were performed using at least three independent biological replicates (independent cultures/extractions). Data are reported as mean ± SD of biological replicates. Statistical analyses were performed on biological replicates. Assumptions were checked using residual analysis and normality testing (Shapiro–Wilk) where applicable; differences were assessed by one-way ANOVA followed by Tukey's *post hoc* test ($p < 0.05$). All graphical outputs were generated with GraphPad Prism 9.0.0.

Results and discussion

Method screening and process rationale

Impact of pre-treatment on inorganic carry-over and extraction selectivity. As a first step, the impact of biomass pre-treatment was assessed, since co-extraction of salts and soluble/loosely associated EPS at this stage can compromise the selectivity of subsequent hydrothermal recovery and bias downstream comparisons. Cyanobacteria of the genus *Chroococcus* are characterised by spherical cells that typically aggregate into small colonies surrounded by a dense mucilaginous B-EPS capsule.[16–19] Maintaining this cell-associated matrix during pre-treatment is important to benchmark selective detachment and purification strategies under a defined starting condition.

Light microscopy suggested that centrifugation removed loosely associated debris while a transparent halo remained visible around many cells (Fig. 2a and b), which is consistent with the presence of an extracellular capsular envelope reported for *Chroococcus* spp.; thus, the halo was used as a qualitative indicator of capsule-associated material. In contrast, gentle washing with distilled water preserved a clearly visible halo around individual cells (Fig. 2c), indicating that washing cycles can reduce loosely associated impurities while maintaining the cell-associated matrix as observed microscopically. Alcian Blue staining (Fig. 2d) provided an additional qualitative readout of acidic polymeric material associated with the biomass, consistent with the presence of an anionic extracellular matrix, and was used to track the redistribution of stained material before and after processing.

SEM analysis supported the microscopy trends. Centrifuged biomass showed less cohesive aggregation and more exposed cell surfaces (Fig. 3a and c), while washed biomass maintained a denser, more cohesive matrix-associated architecture (Fig. 3b and d). These observations are consistent with partial disruption/redistribution of matrix-associated material during centrifugation, whereas washing better preserves the colony-level architecture prior to extraction.

TGA reinforced these findings: centrifuged biomass exhibited significantly higher ash content (74.77 ± 1.97%) than washed samples (66.71 ± 0.02%), indicating greater residual inorganic carry-over. Such contamination can reduce B-EPS purity and is consistent with less effective salt removal at the pre-treatment stage (Fig. S2 and S3).

The structural composition of the biomass and its extracellular matrix was examined by ATR-FTIR spectroscopy (Fig. 4). Spectra were obtained for centrifuged biomass, ultrafiltered B-EPS, and washed biomass. All samples exhibited characteristic absorption bands consistent with polysaccharides and other biomolecular components.[20] A broad band at 3431 cm^{-1} corresponded to the O–H stretching, indicative of hydrogen bonding in carbohydrate-rich materials. Signals near 2976 cm^{-1} were associated with C–H stretching. Bands in the 1600/1380 cm^{-1} region were consistent with carboxylate-containing functionalities, while signals around 1262 cm^{-1} were consistent with sulphate ester contributions. Additional bands at 1063 cm^{-1} (C–O stretching) and 881–625 cm^{-1} were consistent with glycosidic linkages. Overall, FTIR comparisons were used as bulk descriptors to assess whether pre-treatment introduced major changes in functional-group signatures, rather than as definitive structural proof.

Taken together, these complementary analyses indicate that repeated washing reduces inorganic carry-over while maintaining capsule-associated matrix features observed microscopically; therefore, all subsequent extractions employed pre-washed biomass to improve selectivity and comparability across extraction routes.

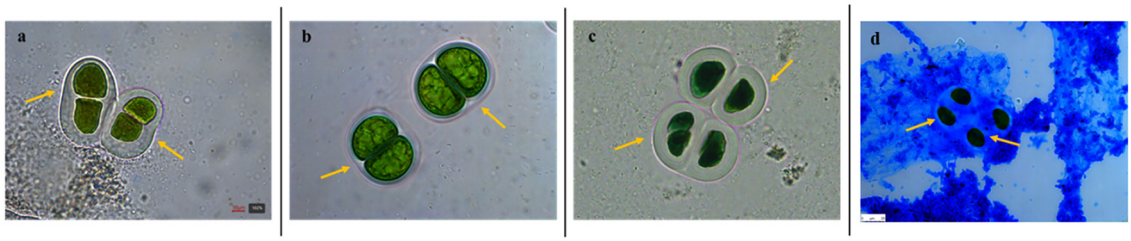

Fig. 2 Light micrographs of *C. submarinus*: (a) untreated biomass; (b) biomass after centrifugation; (c) biomass after three washing cycles; (d) untreated biomass stained with Alcian blue. Images captured at 40× magnification. Yellow arrows indicate a transparent halo around cells, consistent with an extracellular capsular envelope reported for *Chroococcus* spp. and used here as a qualitative indicator.

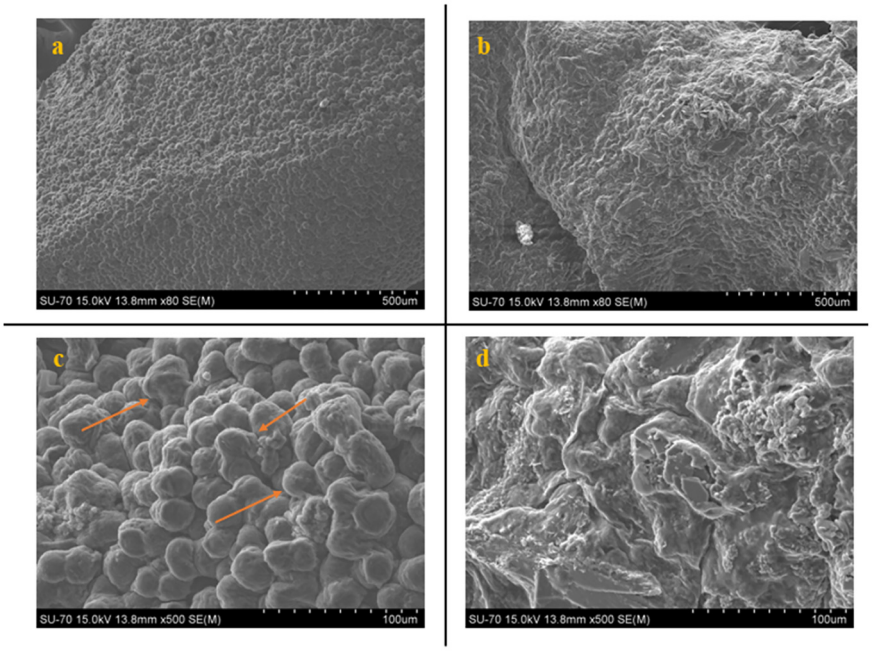

Fig. 3 SEM micrographs of *C. submarinus* biomass after centrifugation (a, 80×; c, 500×) and after three washing cycles (b, 80×; d, 500×). Orange arrows indicate cyanobacterial cells and highlight differences in aggregation and matrix-associated features.

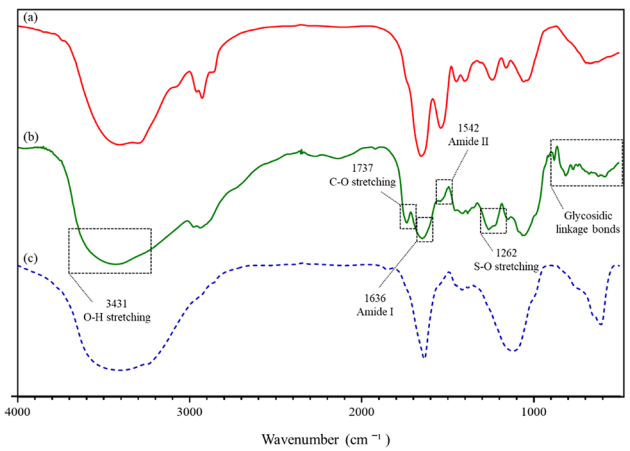

Fig. 4 ATR-FTIR spectra of *C. submarinus* samples: (a) cyanobacterial cells after centrifugation; (b) ultrafiltered B-EPS; (c) biomass after three washing cycles containing both cells and B-EPS.

Hydrothermal extraction–ultrafiltration workflow for B-EPS recovery

Microscopic evidence of matrix disruption. Bright-field micrographs with Alcian Blue showed that all hydrothermal treatments were associated with a marked redistribution of Alcian Blue-stained material from cell-associated regions to the surrounding medium (Fig. 5). Untreated biomass (Fig. 5a) displayed compact *C. submarinus* cells with a pericellular halo, typical of the genus, used here as a qualitative indicator of capsule-associated matrix features.[16,18] After extraction, the halo became less evident in many fields and cells appeared more dispersed, while fields were dominated by diffuse, fibrillar blue-stained material and detached flocs (Fig. 5b–e), consistent with disruption/redistribution of extracellular matrix material under hydrothermal processing. These observations are supported by SEM analysis of biomass after reflux extraction (Fig. 5f), which showed pronounced morphological alterations compared to untreated samples, including changes in aggregation and surface-associated material. Overall, microscopy provides qualitative evidence that hydrothermal processing promotes access to capsule-associated polymeric material across methods, while anticipating method-dependent differences in recovery and inorganic carry-over assessed by orthogonal analytics.[21–23] Visual inspection across the examined fields suggested qualitative, method-dependent patterns. Autoclave-treated samples commonly showed fields dominated by diffuse Alcian Blue-stained material with fewer compact aggregates, whereas reflux and ultrasonication often retained larger aggregates; microwave-treated samples showed heterogeneous fields with both dispersed stained material and residual aggregates.

Ultrafiltration performance: desalting and inorganic carry-over reduction. To ensure comparability among methods, all crude extracts were subjected to UF to remove salts and low-molecular-weight impurities. Beyond its analytical value, UF is a green and scalable alternative to methanol/ethanol precipitation, which typically requires large solvent volumes and can provide incomplete desalting, and is time-consuming. By delivering effective and reproducible desalting under a standardised protocol, UF enabled direct, fair comparisons among hydrothermal methods. Reproducibility was verified by conductivity monitoring over successive UF cycles (Fig. S1), which

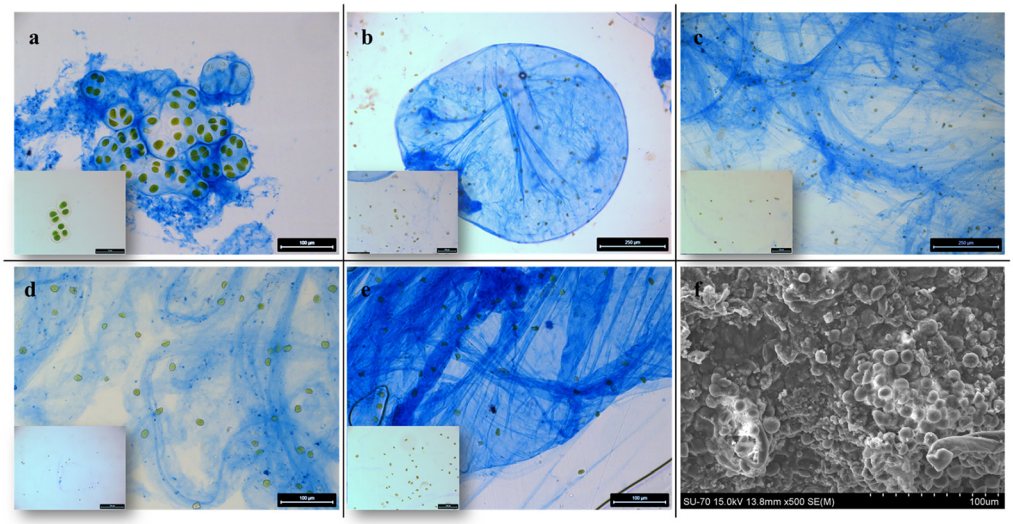

Fig. 5 Bright-field micrographs with Alcian Blue staining of *C. submarinus* biomass before treatment (a, 20×) and after reflux (b, 10×), autoclave (c, 10×), ultrasonic (d, 20×), and microwave (e, 20×) treatments; (f) SEM micrograph of biomass after reflux extraction (f, 500×). Insets (a–e) show higher-magnification views of cells from the corresponding conditions to facilitate visualisation of cell-associated features. Scale bars are shown in each panel.

reached stable plateaus, indicating consistent salt removal across replicates.

The effectiveness of UF was further demonstrated by elemental and ash analysis (Table 1). Across all extraction methods, ash contents decreased by 76–84% relative to pre-UF values, indicating that inorganic salts accounted for a substantial fraction of the initially co-extracted material. A residual ash fraction of 11–18% persisted, which is commonly observed for marine, anionic polysaccharide-rich matrices, because "ash" is not limited to free salts: (i) tightly bound counter-ions (Na^+, Mg^{2+}, Ca^{2+}) can neutralise the negative charges of sulfated and carboxylated groups and yield mineral residues upon combustion (*e.g.*, Na_2SO_4, $CaCO_3$); and (ii) small ions may be retained within hydrated EPS network *via* electrostatic partitioning (Donnan-type retention), reducing dialysability.[23] Further lowering of ash content would likely require additional purification intensity or complementary ion-removal steps, which should be balanced against preservation of polymer properties.

Concomitant with ash reduction, elemental composition became more consistent among extracts after UF, supporting the conclusion that pre-UF differences largely reflected inorganic carry-over. Because post-UF ash levels did not differ significantly among methods (Table 1), the remaining inorganic fraction is consistent with ions associated with the purified B-EPS matrix rather than a method-dependent contaminant. The similar magnitude of ash reduction across methods further indicates that the post-UF B-EPS recovery (Fig. 6) arises predominantly from the variable recovery of the organic B-EPS fraction, rather than from selective salt removal.

Table 1 Elemental analysis and ash content (%), before and after ultrafiltration (UF) of *C. submarinus* B-EPS obtained by different methods

		Elemental analysis					
Extraction		% C	% H	% N	% S	% O[a]	% ashes
Reflux	Before UF	7.463 ± 0.255^{a}	3.179 ± 0.137^{a}	0.505 ± 0.030^{a}	0.000 ± 0.000^{a}	18.025 ± 0.685^{a}	70.720 ± 0.198^{a,b}
	After UF	28.733 ± 0.878^{a}	4.783 ± 0.205^{a}	1.079 ± 0.022^{a}	3.428 ± 0.114^{a}	47.735 ± 1.977^{a,b}	13.415 ± 2.850^{a}
Autoclave	Before UF	10.751 ± 0.675^{b}	3.051 ± 0.165^{a}	0.734 ± 0.074^{b}	1.173 ± 0.121^{b}	17.526 ± 1.424^{a}	68.250 ± 3.026^{a}
	After UF	28.689 ± 0.131^{a}	4.576 ± 0.387^{a}	1.070 ± 0.052^{a}	3.437 ± 0.225^{a}	50.397 ± 1.249^{a}	11.205 ± 1.379^{a}
Ultrasonic	Before UF	4.440 ± 0.156^{c}	1.469 ± 0.126^{b}	0.418 ± 0.003^{a,c}	1.061 ± 0.109^{b}	16.153 ± 1.589^{a}	75.190 ± 3.917^{b}
	After UF	28.963 ± 0.055^{a}	4.866 ± 0.212^{a}	1.214 ± 0.005^{a}	3.473 ± 0.404^{a}	45.403 ± 0.846^{b}	17.615 ± 2.058^{a}
Microwave	Before UF	2.937 ± 0.233^{d}	2.656 ± 0.174^{c}	0.363 ± 0.024^{c}	1.068 ± 0.060^{b}	12.076 ± 0.659^{b}	80.665 ± 0.757^{b}
	After UF	30.750 ± 0.528^{a}	5.555 ± 0.343^{a}	1.162 ± 0.064^{a}	1.214 ± 0.130^{b}	48.576 ± 2.666^{a,b}	12.720 ± 3.224^{a}

[a] Calculated value % O = 100 − (% C + % H + % N + % S + % ash). Different letters represent significantly different means of the different extraction methods (p-value ≤0.05).

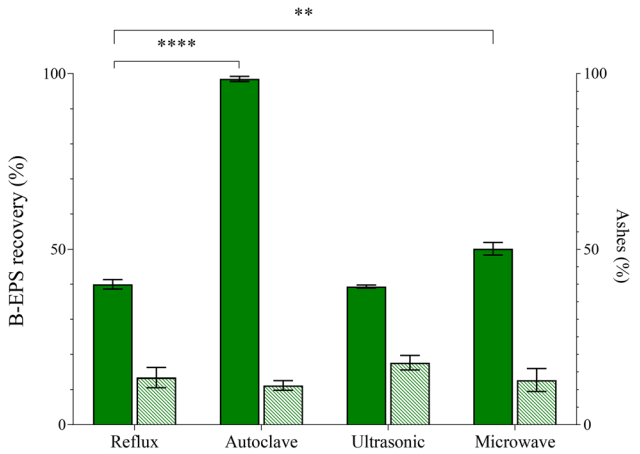

Fig. 6 B-EPS recovery and ash content after ultrafiltration from *C. submarinus* using different extraction methods. (**) $p < 0.01$ and (****) $p < 0.0001$ indicate statistically significant differences compared with the standard method (reflux). Ash content did not differ significantly among methods.

Accordingly, method-dependent yield contrasts were interpreted together with orthogonal bulk descriptors (ATR-FTIR, TGA, and zeta potential) rather than microscopy alone.

B-EPS recovery. After UF, the dry mass recovered in the UF-retained fraction highlighted clear differences among the hydrothermal methods (Fig. 6). Autoclave extraction provided the highest recovered mass, corresponding to up to 2.5-fold higher recovery than reflux or ultrasonic treatments. Under the tested conditions, this indicates higher recovery of the UF-retained polymer-rich fraction operationally associated with B-EPS, consistent with reports where pressurised hydrothermal processing improved recovery of cell-associated EPS.[4,21] Because the post-UF ash content did not differ significantly among methods (Fig. 6), the higher recovered mass is most parsimoniously interpreted as reflecting enhanced recovery of the organic fraction, rather than differences in residual inorganic carry-over.

Microwave extraction achieved intermediate recovery (*ca.* 50% relative recovery), showing improved performance compared with reflux/ultrasonic under the conditions applied. As a domestic microwave system was used, the resulting treatment is best regarded as a comparative, partially controlled condition, since spatially heterogeneous dielectric heating can introduce variability in the effective thermal history experienced by the suspension.

Ultrasonic extraction yielded the lowest recovery (*ca.* 40%) and showed no statistically significant improvement over reflux. Although ultrasonication has been reported to increase cell permeability and enhance mass transfer,[22] under the present operating window (bath mode, 80 °C, 15 min) this effect did not translate into increased recovery of the cell-associated fraction. The recovered material may therefore reflect preferential release of more loosely associated extracellular material rather than efficient detachment of the tightly cell-bound matrix, consistent with the limited increase in recovery (%).

Overall, the recovery differences reflect method-dependent extraction efficiency of the B-EPS fraction. Since UF removed ionic contaminants to comparable post-UF levels across methods (Fig. 6), the observed contrasts primarily reflect differences in each treatment's ability to mobilise cell-associated matrix material into the extractable fraction. Within the conditions screened, autoclave extraction delivered the highest B-EPS recovery and is compatible with solvent-free downstream purification by UF, supporting its selection for subsequent multivariate optimisation.

Chemical and physicochemical evaluation of the B-EPS extracted

ATR-FTIR. B-EPS recovered by the four hydrothermal methods were characterised by an integrated suite of analyses (elemental composition, ATR-FTIR, zeta potential, and TGA). As all extracts were subjected to the same UF workflow, the ensuing measurements are less influenced by free salts and low-molecular-weight species and are therefore discussed primarily in the context of the extraction conditions within this harmonised protocol.

After UF, the elemental profiles became broadly comparable across methods, with carbon stabilising at 28–31%, nitrogen at 1.1–1.2%, and sulfur at 1.2–3.4% (Table 1). This convergence supports the interpretation that the greater pre-UF variability was driven predominantly by method-dependent inorganic carryover rather than by intrinsic compositional differences in the purified polymer fraction. ATR-FTIR spectra (Fig. 7) consistently showed a broad O–H stretch (3200–3500 cm^{-1}); carboxylate (COO^-) bands (ν_{as} at 1600–1550 cm^{-1} and ν_s at 1400–1300 cm^{-1}); sulfate esters (S=O, 1262 cm^{-1}); intense carbohydrate C–O/C–O–C stretches (1150–1000 cm^{-1}); glycosidic/anomeric modes (881–625 cm^{-1}); and amide I/II (1636/1542 cm^{-1}). Overall, the spectra largely overlapped across

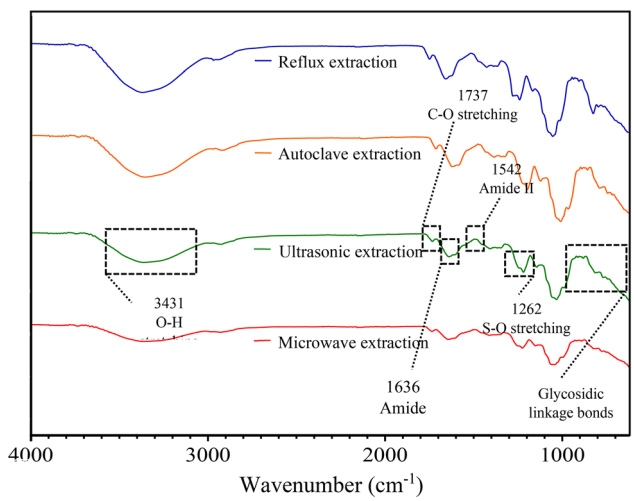

Fig. 7 ATR-FTIR spectra of *C. submarinus* B-EPS after various extraction methods following ultrafiltration.

Table 2 Zeta potential of *C. submarinus* B-EPS after ultrafiltration obtained, obtained by different extraction methods

Extraction	Zeta potential (mV)
Reflux	−46.4 ± 3.4[a]
Autoclave	−49.9 ± 2.7[a]
Ultrasonic	−30.9 ± 2.9[b]
Microwave	−33.9 ± 3.5[b]

Different letters represent significantly different means ($p \leq 0.05$).

methods, with only modest intensity differences in selected regions; such variations may reflect differences in the relative contribution of proteinaceous components and/or residual ion-polymer associations, rather than unequivocal loss of functional groups.

Zeta potential. Measurements of surface charge (Table 2) further distinguished the methods. Autoclave and reflux extractions showed highly negative zeta potentials (−49.9 to −46.4 mV), compatible with a higher apparent availability of anionic functionalities (carboxylate/sulphate) inferred from ATR-FTIR. In contrast, ultrasonic and microwave extracts showed significantly less negative values (−30.9 to −33.9 mV), which may indicate partial shielding of anionic sites and/or differences in ion association within the purified matrix. Because zeta potential is sensitive to ionic strength, the values are interpreted as comparative screening descriptors: all samples were measured after UF and diluted to a comparable conductivity range under identical aqueous conditions. For context, these zeta potentials values are more negative than those commonly reported for several bacterial EPS under aqueous conditions[21,22] and are consistent with strong electrostatic stabilisation of these dispersions under the applied measurement conditions.

Thermogravimetric analysis (TGA). TGA showed broadly comparable thermal degradation patterns across the purified B-EPS extracts. A major mass-loss region was observed between 100–550 °C, with a dominant event centred at 245–265 °C, and a residual mass (ash) in the 11–20% range (Fig. 8). Differences among curves were modest within the comparative framework of this study, supporting overall similarity in bulk thermal behaviour across extraction routes. These results are consistent with previous reports describing comparable pyrolysis behaviour of microbial EPS within comparable temperature ranges.[24,25]

Taken together, these results indicate that autoclave and reflux extraction produced B-EPS with the most similar bulk signatures across elemental analysis/ATR-FTIR and the most negative zeta potential values, while maintaining comparable thermal behaviour. Ultrasonic and microwave extractions also enabled recovery of B-EPS, but showed less negative zeta potential values and modest differences in FTIR band intensities, which may reflect differences in ion association and/or relative matrix composition within the purified fraction under the tested conditions.

Further work will extend the structural characterisation to monosaccharide composition, molecular-weight distribution, and NMR to strengthen structure–function interpretation and support application-driven material design.

Multivariate optimisation of autoclave extraction by RSM

Model scope and design. The autoclave extraction method was selected for optimisation since it provided the highest recovery and showed no major changes in bulk signatures across the applied analytics in the comparative analyses. To refine this method, RSM was applied as a multivariate statistical tool capable of identifying interactions among variables that would be overlooked in a one-factor-at-a-time approach. The experimental design evaluated three independent factors: biomass-to-solvent ratio (1 : 5–1 : 20 (w/v)), temperature (108–134 °C), and extraction time (5–25 min) (Table S2). Overall, the RSM model provided a satisfactory fit, as reflected by small-to-moderate prediction deviations for most experimental runs, with a limited number of higher-deviation points (Table S2). Accordingly, downstream comparisons were based on both recovery and orthogonal bulk descriptors (ash/elemental content, ATR-FTIR, TGA, and zeta potential), rather than microscopy alone. This systematic approach generated predictive models to identify optimal conditions for maximising

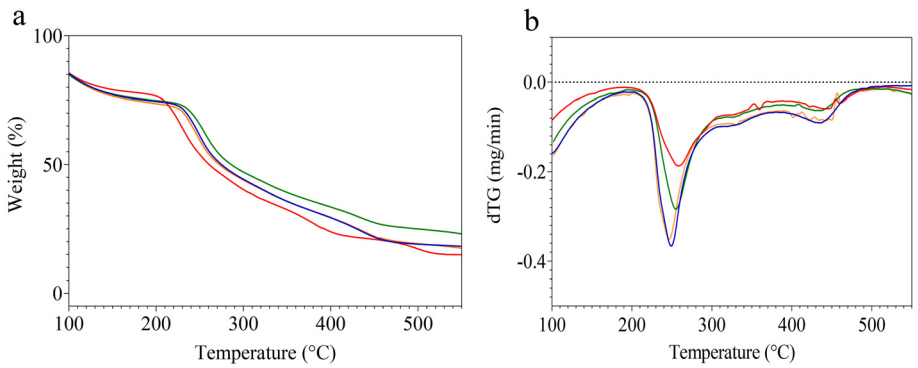

Fig. 8 TGA (a) and dTG (b) of *C. submarinus* B-EPS after various extraction methods following ultrafiltration: reflux (blue line), autoclave (orange line), ultrasonic (green line) and microwave (red line).

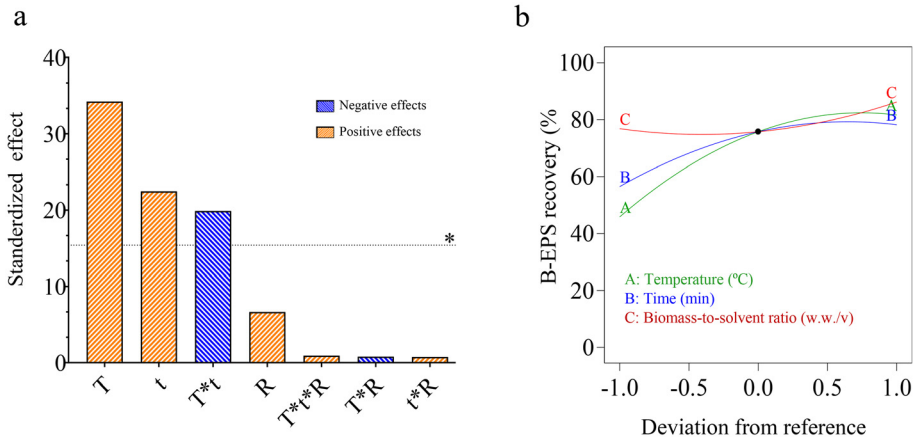

Fig. 9 Pareto chart on the degree of influence of the independent variables in determining the recovery of B-EPS of *C. submarinus* using the autoclave method. The horizontal line represents the threshold of statistical significance. *T*: temperature (°C); *t*: time (min); *R*: biomass-to-solvent ratio (w/v) (a). Perturbation plot for B-EPS recovery (%) (b).

recovery under water-based, solvent-free processing, avoiding solvent precipitation and hazardous reagents.

Main effects and response surfaces. The influence of individual variables on B-EPS recovery (%) was assessed through statistical analysis and visualised using the Pareto chart (Fig. 9a). Among the tested factors, temperature emerged as the most significant variable, followed by extraction time, both exceeding the threshold of statistical significance. The perturbation plot (Fig. 9b) confirmed these findings, showing steep, positive slopes for temperature (*A*) and time (*B*), whereas the biomass-to-solvent ratio (*C*) exerted only a minor effect. Within the studied window, higher temperature and longer extraction time were therefore associated with increased B-EPS recovery, whereas the biomass-to-solvent ratio had a comparatively smaller contribution.

The combined effects of temperature and time were further visualised through the 3D response surface plot (Fig. 10a). The contour mapping showed that increasing both parameters simultaneously resulted in higher B-EPS recovery within the studied processing window, whereas the biomass-to-solvent ratio produced comparatively smaller changes in the response.

Model fitting and diagnostics. Statistical validation by ANOVA confirmed the robustness of the model, with a high *F*-value (94.37), $p < 0.0001$, and no significant lack-of-fit ($p \geq 0.05$), supporting its use for prediction within the investigated design space. The precision and predictive capacity of the model across the design space were assessed through the Fraction of Design Space (FDS) analysis (Fig. 10b). The model achieved a desirability of 1.0 and an FDS of 0.50, indicating that half of the design space meets the predefined precision criterion. Furthermore, a standard error (SE) of 0.33 indicated that 50% of the design space maintained SE ≤ 0.33, consistent with relatively uniform prediction precision across the explored region. Model performance was also evaluated by comparing predicted and experimental responses; the predicted *versus* experimental plot (Fig. 10c) showed an absence of obvious systematic patterns, supporting the robustness of the regression model.

Regression equation and validation. The regression equation describing the relationship between the recovery and the independent variables is shown in eqn (1):

$$\begin{aligned}\text{B-EPS recovery}(\%) = {} & \\ & -1273.738 + 19.807 \times T + 14.070 \times t - 7.039 \times R \\ & - 0.090 \times T \times t + 0.006 \times T \times R + 0.024 \times t \times R \\ & - 0.071 \times T^2 - 0.0839 \times t^2 + 0.231 \times R^2.\end{aligned} \quad (1)$$

This model allows prediction of B-EPS recovery within the studied design space. Model adequacy was supported by the agreement between predicted and experimental responses and by residual diagnostics (Fig. 10c and d). Model predictions were additionally verified (Table S3) against independent temperature–time combinations and the predicted optimum, showing mostly low-to-moderate relative deviations, with a few larger deviations at specific design points (up to 18% in Table S2) within the studied processing window. Under the optimised conditions (R = 1 : 20 g mL^{-1}, T = 130 °C, t = 16 min), the model predicted 93.62%, and the experimental recovery was 91.59% (relative deviation 2.3%).

Collectively, these results highlight RSM as a useful tool for optimising water-based extraction processes by enabling multivariable optimisation and prediction within a defined processing window. By refining autoclave parameters, the method achieved high recovery under solvent-free conditions, supporting its potential for scale-relevant processing. The integration of hydrothermal extraction with UF avoids solvent precipitation and enables desalting without organic solvents, providing an operationally simple route to purified B-EPS suitable for downstream characterisation and materials-oriented evaluation.

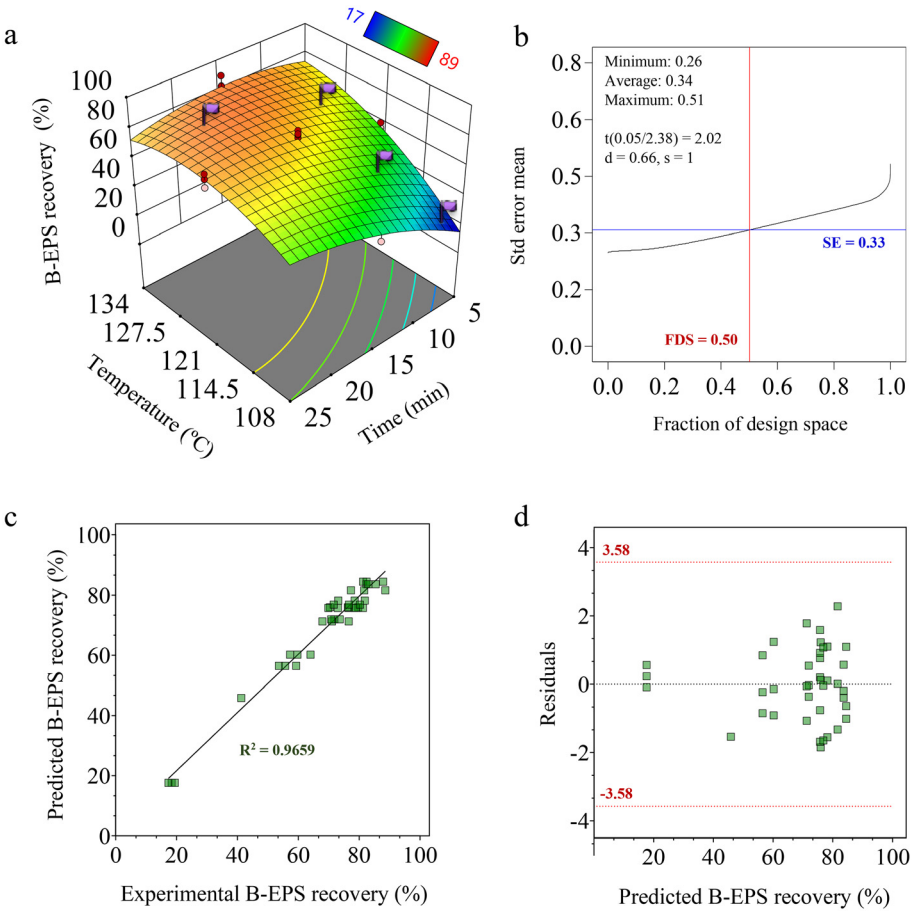

Fig. 10 3D response surface plot of B-EPS recovery as a function of temperature and time (a). Purple flags – experimentally-confirmed values. Fraction of Design Space (FDS) (SE-standard error of the mean; *t*-tolerance value; 95% confidence interval; *d*-half-width of the prediction interval; and *s*-standard deviation of the model's predictions) (b). Comparison between predicted response and experimental response (c). Residual plot for predicted *versus* experimental responses (d).

Sustainability and techno-economic assessment

A credible green route to B-EPS requires not only high technical recovery but also a low environmental footprint and realistic costs. The hydrothermal extraction followed by workflow developed here aligns with Green Chemistry principles by using water as the sole processing medium, eliminating organic solvents and added reagents, and minimising waste.

Environmental performance. Autoclave extraction employs saturated steam and short residence times to promote detachment of cell-associated B-EPS. Potential differences in energy demand among extraction methods were evaluated using first-order, device-level indicators based on rated power and treatment time (Table S4). These estimates are intended for within-study benchmarking and do not represent a full process energy balance; therefore, energy considerations are interpreted alongside recovery, desalting performance, and solvent avoidance. Importantly, coupling the extraction step with UF for desalting replaces conventional alcohol precipitation, thereby eliminating the use of organic solvents and the generation of solvent-derived waste streams. Consistent with Table 1, UF removes the bulk of co-extracted ions (76–84% ash reduction), enabling purified polymers without solvent precipitation. The UF permeate is an aqueous stream dominated by salts and low-molecular-weight solutes; its potential reuse as process water would require case-by-case evaluation (*e.g.*, conductivity limits, fouling/bioburden control). Overall, the workflow prioritises waste prevention and safer processing media (water), while allowing future integration of heat/water recirculation strategies where technically justified.

Economic viability. Although pressurised vessels entail upfront CAPEX, autoclaves and UF skids are standard, off-the-shelf equipment, lowering adoption barriers. OPEX may benefit from avoiding solvent purchase, handling and recovery, short cycle times (RSM-optimised), and high recovery, which can reduce the upstream biomass required per unit of B-EPS. No cost estimates are claimed here; this section outlines first-order drivers to be quantified in future TEA using site-specific utilities, batch loading, and membrane lifetime data. Operating costs are expected to be driven by steam/electricity and periodic membrane replacement; these contributions can be quantified in future TEA using site-specific utilities, batch

loading, and membrane lifetime data. The batch nature of autoclaves supports modular scale-up and flexible scheduling, facilitating incremental capacity increases and integration into existing microalgae platforms.

Circular-bioeconomy fit. Integration with photosynthetic cultivation platforms may support circular-bioeconomy strategies. Residual biomass from extraction (cells, proteins, pigments) remains available for co-product valorisation, improving overall resource efficiency. The resulting desalted/purified (reduced-ash) B-EPS may support the development of biobased coatings/films and functional biomaterials, advancing the replacement of fossil-derived plastics.

Implementation of metrics. For scale-up and certification, future work should track *E*-factor, process mass intensity (including water PMI), energy intensity (kWh kg^{-1} B-EPS), GHG intensity (kg CO_2e kg^{-1}), membrane life/cost per kg product, and cost of goods. In the present study, Table 1 (salt removal by UF), Fig. 6 (post-UF recovery/ash), and Table S4 (equipment-level energy indicators for the extraction step) provide a first quantitative basis to support prospective TEA/LCA.

First-order energy and material-efficiency metrics. To support the sustainability discussion, a first-order estimate of specific energy input was calculated for each device based on its rated power and the effective treatment time under the tested conditions (Table S4). This equipment-level indicator is intended for within-study benchmarking of extraction strategies and does not represent a full process energy balance. Specific energy input was normalised by the mass of purified B-EPS recovered per batch resulting in kWh g^{-1} of purified B-EPS recovered for benchmarking of extraction strategies. In addition, a simplified PMI/*E*-factor perspective was considered, highlighting that the hydrothermal + UF workflow avoids organic solvent precipitation and associated solvent waste streams.

Overall, the autoclave + UF route combines high recovery with effective solvent-free desalting and provides a promising basis for future TEA/LCA and application-driven scale-up evaluation.

Conclusions

This work demonstrates a solvent-free hydrothermal-ultrafiltration workflow for recovering bound extracellular polymeric substances (B-EPS) from the marine cyanobacterium *Chroococcus submarinus*, avoiding hazardous reagents and solvent precipitation. The extracts showed reduced inorganic carry-over and no major changes in the assessed bulk signatures across the applied analytics, supporting the potential for scale-relevant processing. Overall, the proposed hydrothermal extraction followed by ultrafiltration framework offers a scale-relevant, industrially compatible route to producing microbial polysaccharide materials within CO_2-fixing, seawater-based cultivation systems and circular bio-based materials development. Future work will focus on advanced structural characterisation and life-cycle assessment to strengthen structure–function understanding and quantify environmental performance at scale.

Conflicts of interest

There are no conflicts to declare.

Data availability

The data supporting this article are provided in the supplementary information (SI). Supplementary information: ASP-12 medium composition (Table S1), the RSM central composite design matrix with model-predicted responses (Table S2), the external validation runs (Table S3), ultrafiltration conductivity monitoring (Fig. S1), thermogravimetric data for biomass/crude extracts (Fig. S2 and S3), and first-order equipment-level energy/material-efficiency indicators for the extraction step (Table S4). See DOI: https://doi.org/10.1039/d6gc00485g.

Acknowledgements

This research was supported by the European Territorial Cooperation Programme Interreg MAC 2021-2027 through the CALYPSO project (1/MAC/1/1.1/0088). CIIMAR was funded by the Foundation for Science and Technology (FCT) through UID/04423/2025, UID/PRR/04423/2025, and LA/P/0101/2020. Ivana Mendonça, Filipa Rodrigues, and Marisa Faria were financially supported by FCT doctoral grants (2023.04389.BD, 2024.01262.BD, and 2020.06615.BD, respectively).

References

1 H. A. H. Ibrahim, H. E. Abou Elhassayeb and W. M. M. El-Sayed, *J. Genet. Eng. Biotechnol.*, 2022, **20**, 151, DOI: 10.1186/s43141-022-00432-2.
2 D. Kumar, P. Kastanek and S. P. Adhikary, *Curr. Sci.*, 2018, **115**, 234, DOI: 10.18520/cs/v115/i2/234-241.
3 J.-C. Kehr and E. Dittmann, *Life*, 2015, **5**, 164–180, DOI: 10.3390/life5010164.
4 Z. Li, G. Dai, P. Juneau and B. Qiu, *J. Phycol.*, 2016, **52**, 105–115, DOI: 10.1111/jpy.12372.
5 S. Raungsomboon, A. Chidthaisong, B. Bunnag, D. Inthorn and N. W. Harvey, *Water Res.*, 2006, **40**, 3759–3766, DOI: 10.1016/j.watres.2006.08.013.
6 C. Laroche, *Mar. Drugs*, 2022, **20**, 336, DOI: 10.3390/md20050336.
7 Y. Huang, H. Chen, K. Zhang, Y. Lu, Q. Wu, J. Chen, Y. Li, Q. Wu and Y. Chen, *Int. J. Biol. Macromol.*, 2022, **213**, 967–986, DOI: 10.1016/j.ijbiomac.2022.06.049.
8 S. Rodriguez, F. G. Torres and D. López, *Polym. Renewable Resour.*, 2017, **8**, 133–150, DOI: 10.1177/204124791700800401.

9 O. N. Tiwari, M. Muthuraj, B. Bhunia, T. K. Bandyopadhyay, K. Annapurna, M. Sahu and T. Indrama, *Polym. Test.*, 2020, **89**, 106592, DOI: 10.1016/j.polymertesting.2020.106592.
10 D. Cruz, V. Vasconcelos, G. Pierre, P. Michaud and C. Delattre, *Appl. Sci.*, 2020, **10**, 3763, DOI: 10.3390/app10113763.
11 C. Delattre, G. Pierre, C. Laroche and P. Michaud, *Biotechnol. Adv.*, 2016, **34**, 1159–1179, DOI: 10.1016/j.biotechadv.2016.08.001.
12 S. Singh, C. Kant, R. K. Yadav, Y. P. Reddy and G. Abraham, in *Cyanobacteria*, Elsevier, 2019, pp. 347–358. DOI: 10.1016/B978-0-12-814667-5.00017-9.
13 F. Rodrigues, I. Mendonça, M. Faria, J. L. Gómez Pinchetti, A. Ferreira and N. Cordeiro, *Chemosphere*, 2025, **393**, 144759, DOI: 10.1016/j.chemosphere.2025.144759.
14 I. Mendonça, J. Sousa, C. Cunha, M. Faria, A. Ferreira and N. Cordeiro, *Chemosphere*, 2022, **314**, 137719, DOI: 10.1016/j.chemosphere.2022.137719.
15 F. Rodrigues, I. Mendonça, M. Faria, R. Gomes, J. L. G. Pinchetti, A. Ferreira and N. Cordeiro, *Processes*, 2024, **12**, 1733, DOI: 10.3390/pr12081733.
16 C. Duval, S. Hamlaoui, B. Piquet, G. Toutirais, C. Yéprémian, A. Reinhardt, S. Duperron, B. Marie, J. Demay and C. Bernard, *FEMS Microbes*, 2021, **2**, xtab006, DOI: 10.1093/femsmc/xtab006.
17 W. A. Gama, J. Rigonato, M. F. Fiore and C. L. Sant'Anna, *Eur. J. Phycol.*, 2019, **54**, 315–325, DOI: 10.1080/09670262.2018.1563913.
18 W. K. Hofbauer and G. Gärtner, *Microbial life on Façades*, Springer Berlin Heidelberg, Berlin, Heidelberg, 2021. DOI: 10.1007/978-3-662-54833-2.
19 B. Nowruzi and F. Soares, *Int. J. Syst. Evol. Microbiol.*, 2021, **71**, 004828, DOI: 10.1099/ijsem.0.004828.
20 V. Nóbrega, M. Faria, A. Quintana, M. Kaufmann, A. Ferreira and N. Cordeiro, *Materials*, 2019, **12**, 2275, DOI: 10.3390/ma12142275.
21 X. Yang, Y. Ren and L. Li, *LWT – Food Sci. Technol.*, 2022, **153**, 112345, DOI: 10.1016/j.lwt.2021.112345.
22 D. Zhao, J. Jiang, L. Liu, S. Wang, W. Ping and J. Ge, *Int. J. Biol. Macromol.*, 2021, **178**, 306–315, DOI: 10.1016/j.ijbiomac.2021.02.182.
23 F. Miao, A. Velayudhan, E. DiBella, J. Shervin, M. Felo, M. Teeters and P. Alred, *Biotechnol. Prog.*, 2009, **25**, 964–972, DOI: 10.1002/btpr.168.
24 K. B. Solmaz, Y. Ozcan, N. Mercan Dogan, O. Bozkaya and S. Ide, *Environments*, 2018, **5**, 63, DOI: 10.3390/environments5060063.
25 A. T. Koçer, B. İnan, S. Kaptan Usul, D. Özçimen, M. T. Yılmaz and İ. Işıldak, *Braz. J. Microbiol.*, 2021, **52**, 1779–1790, DOI: 10.1007/s42770-021-00575-3.